Polycrystalline tetrabenzoporphyrin organic field-effect transistors with nanostructured channels

Patrick B. Shea,[a] Charlene Chen, and Jerzy Kanicki[b]
Organic and Molecular Electronics Laboratory, Department of Electrical Engineering and Computer Science, The University of Michigan, Ann Arbor, Michigan 48109

Lisa R. Pattison and Pierre Petroff
Department of Materials Science and Engineering, The University of California, Santa Barbara, California 93106

Hiroko Yamada and Noboru Ono
Department of Chemistry in the Faculty of Science, Ehime University, Bunkyo-cho 2-5, Matsuyama 790-8577, Japan

(Received 13 January 2007; accepted 9 May 2007; published online 5 June 2007)

Solution-processed organic thin-film field-effect transistors (OFETs) were fabricated using a precursor form of the organic semiconductor tetrabenzoporphyrin (TBP) deposited on a thermal silicon oxide gate insulator patterned with nanometer-scale trenches. Thermal conversion of the precursor film to TBP was enhanced by ordered TBP aggregation in the prepatterned trenches, demonstrating precise control and placement of long- and short-range ordering of the organic semiconductor. OFETs with channels parallel to trench direction growth were found to have field-effect mobility approaching one order of magnitude greater than transistors fabricated with the channel oriented perpendicular to dendrimer growth. © *2007 American Institute of Physics*.
[DOI: 10.1063/1.2745227]

Advancement in organic thin-film field-effect transistor (OFET) technology has typically focused on development of organic materials with high charge carrier field-effect mobility (μ_{FE}) or solution processability.[1] Alteration of the gate insulator surface itself has been mostly confined to surface modification using self-assembled monolayers.[2] Some works have reported increased molecular ordering in organic semiconductor thin films when the substrates are directionally rubbed before semiconductor deposition,[3–5] concluding that the rubbing induces ridging on the substrate surface leading to increased polymer or small molecule ordering. An alternate methodology for enhanced ordering organic thin films is graphoepitaxy, wherein a substrate is patterned as a template to enhance crystallization of its coating.[6] van de Craats *et al.* reported OFETs utilizing mesoepitaxial ordering of liquid-crystalline polymers deposited from solution onto oriented poly(tetrafluoroethylene) substrates,[7] wherein discotic liquid-crystalline polymers self-aligned into columnar stacks following solution casting and slow solvent evaporation.

Tetrabenzoporphyrins (TBPs) have been demonstrated as feasible materials for OFETs processed from solution and forming polycrystalline thin films.[8–11] TBPs are synthesized in a soluble precursor form that upon solution deposition is amorphous and insulating.[12–14] During thermal annealing, the precursor molecule converts to an insoluble, planar molecule that forms polycrystalline, semiconducting thin films. During the thermal conversion process TBP molecules aggregate into ordered rods,[11] or in the case of sparsely deposited metal-free TBP, into dendritic, fractal clusters.[15] Aggregation in porphyrins is typically observed as fractal or ordered in structure, with aggregation being a reaction-limited, diffusion limited, or diffusion-limited cluster-cluster mechanism, or a combination of mechanisms.[16–19] In this work, the molecular thermal conversion process is exploited by prepatterning the gate dielectric surface to allow for templated crystallization of TBP aggregates. Periodic, rectangular patterns were formed in a SiO_2 (gate insulator) surface using laser interference lithography.[20] Upon thermal conversion, long-range-ordered TBP aggregation was observed in the substrate trenches, and OFETs fabricated from these films demonstrated field-effect mobility anisotropy with trench orientation with respect to the device channel direction.

OFETs were fabricated on highly doped (n^{++}) crystalline silicon substrates with a 200-nm-thick thermal oxide layer as the substrate, gate dielectric, and gate electrode (Fig. 1). Pristine substrates were cleaned by rinsing with acetone, isopropyl alcohol, and de-ionized water, then baked to remove solvent. Following spin coating of hexamethyldisilazane and photoresist, laser-interference lithography[20] was used to expose the sample. Following photoresist development, the substrates were etched in inductively coupled plasma. Square-wave trenches were etched into the SiO_2. The precursor tetrabicycloporphyrin (CP) was dissolved in chloroform (0.7 wt. %), then spun cast onto the cleaned substrates in N_2. Thin-film deposition was followed by thermal conversion of the CP thin film to TBP by baking in vacuum at 180 °C for 30 min. OFETs were then completed by thermal evaporation of Au through a stencil mask to form staggered source and drain electrodes. OFETs were tested in air and in the dark using a Hewlett-Packard 4156A semiconductor parameter analyzer, with electrical contact to the gate electrode made using indium-gallium eutectic. The effect of the trenches on the gate capacitance (C_i) was found to be negligible, whereas variation in the transistor channel dimensions was non-negligible and included in OFET analysis. The calculated gate capacitance used in extracting OFET properties was 1.74×10^{-8} F/cm^2. Parameters such as μ_{FE} and the accumu-

[a]URL: htpp://www.eecs.umich.edu/omelab
[b]Electronic mail: kanicki@eecs.umich.edu

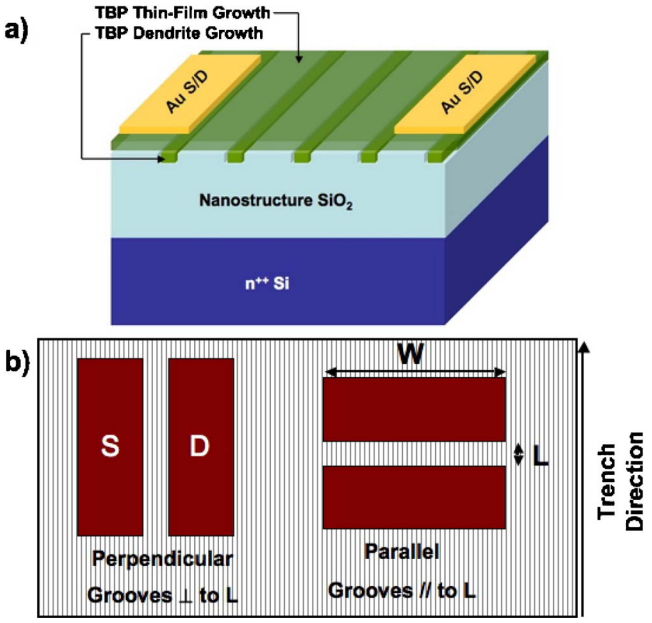

FIG. 1. (Color online) (a) Schematic cross section of nanostructured TBP OFETs. (b) Top-view schematic of nanostructured OFETs structures.

lation threshold voltage (V_T) were extracted from the transfer characteristics in the linear regime ($|V_{DS}| < |V_{GS}-V_T|$) using a previously described nonlinear curve fitting method that attempts to account for dispersive charge transport.[21]

Fractal and micrometer-scale ordered nanorod aggregation are both observed in precursor-route TBP thin films deposited on unpatterned, bare SiO_2, as shown in Figs. 2(a) and 2(b). Thinner regions of the same film, with more sparse surface coverage density, display fractal aggregation [Fig. 2(a)]. For thin films with higher surface coverage density [Fig. 2(b)], nanorod-type aggregation is predominant, with the nanorods orienting relative to each other to form micrometer-sized domains.[8] Typical TBP rod-shaped aggregates demonstrate widths of 60 nm and lengths of 300 nm. The change in aggregation structure with surface coverage density may be explained by a variation in molecular surface mobility. When porphyrin aggregates are more mobile, such as on bare SiO_2 with sparse surface coverage density, significant branching in aggregation is favorable and fractal growth occurs. Conversely, a higher surface coverage density, such as when the precursor thin film is thick, limits aggregate diffusion, inducing ordered rodlike growth rather than disordered dendritic growth. As yet, intermediate stages of thermal conversion have not been been studied with AFM to determine the specific aggregation mechanism.

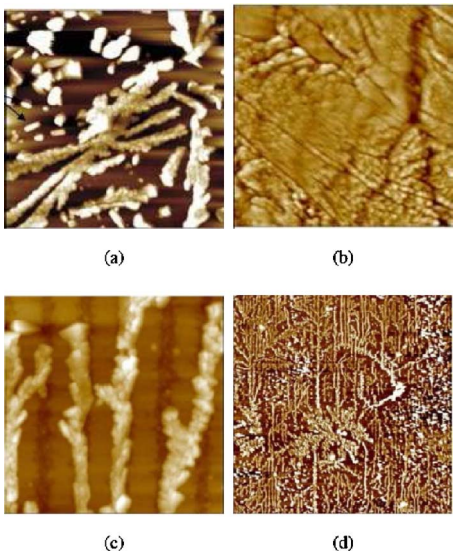

FIG. 2. (Color online) AFM height micrographs of (a) fractal aggregation of sparse, solution-processed TBP; (b) aligned domain formation in more dense TBP; (c) a close view of TBP aggregation within trenches; and (d) a wider-scale view of TBP aggregation wire formation within trenches. The axes dimensions are (a) 3 μm, (b) 2 μm, (c) 2.2 μm, and (d) 25.2 μm. Samples in (c) and (d) have a trench periodicity of 450 nm and a trench depth of 10 nm.

The SiO_2/n^{++}-*c*-Si substrates with large-area topographic periodic modulation defined by laser interference lithography described here were fabricated with square-wave trenches with depths ranging from 10 to 40 nm, widths of 100 nm, and periodicities varying from 200 to 460 nm. The best dimensions observed for preferred molecular alignment were obtained for substrates with a nanogroove periodicity of 460 nm and depth of 40 nm, corresponding to an aspect ratio (width to height) of about 10.[22] Grooves with smaller periodicity appear to prevent nucleation within the trenches, and crystals instead are formed randomly on the top surfaces of the grooves. The height should be large enough to induce molecular orientation, but small enough to prevent film roughness. The structural studies were performed to optimize the periodic structures to achieve uniformly oriented thin films; OFETs were only fabricated over optimized square-wave gratings. AFM height micrographs of TBP nanowire formations in sparse regions of the TBP thin film are shown in Figs. 2(c) and 2(d). The axis scale in Fig. 2(c) is 2.2 μm, with the nanoindentations appearing as the darker areas in the image background. Upon thermal conversion of the precursor, TBP demonstrates preferential alignment along the trench direction. The SiO_2 topography appears to limit lateral mobility of the TBP clusters, causing them to grow along the trench direction, with continuous lengths up to 10 μm, giving a dimensional anisotropy ratio of 100 with aggregation being approximately 100 nm wide. Lateral connections of TBP aggregates in neighboring trenches are observed, as well as jumping of aggregates from one trench to another. In Fig. 2(c), TBP aggregation appears to be of dendritic nature, rather than the more massive single nanorod growth observed in NiTBP.[10] AFM imagery of the sparse films also indicates that TBP crystallization in the trenches can be considered a distinct process from crystallization in the bulk TBP, or in TBP without a structured SiO_2 surface. That is, the entire thin film comprises a polycrystalline layer within the trenches with crystallite sized limited by the trench dimensions and a polycrystalline layer with larger grain sizes limited by the surface mobility of TBP aggregates.

TBP OFETs were fabricated with the channel lengths (L) parallel and perpendicular to the trenches. Devices were fabricated with a range of channel width (W) to length ratios (W/L) to determine if source and drain electrode contact resistance factored on observed OFET field-effect mobility anisotropy with nanowire orientation; thus, all OFET electrical characteristics are shown normalized to W/L. However, contact resistance was not observed to have a considerable effect. Electrical characteristics for OFETs of both parallel and perpendicular orientation of the channel to the trench direction are shown in Figs. 3 and 4. The presence of the trenches was found to increase the effective OFET W by

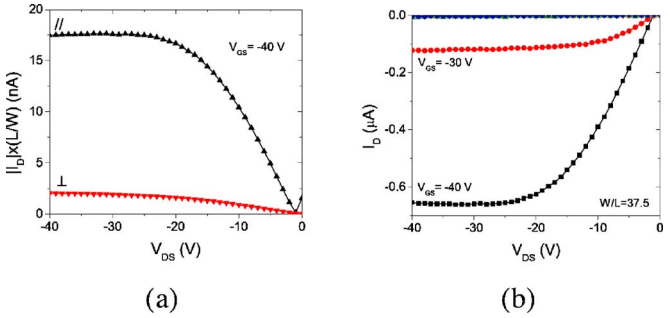

FIG. 3. (Color online) (a) Output characteristics of TBP OFETs with trenches aligned parallel (||) and perpendicular (⊥) to the channel length at $V_{GS}=-40$ V. I_D for both devices has been normalized to W/L, revealing anisotropy with trench direction. (b) Output characteristics of a TBP OFET on nanostructured SiO_2 with trenches aligned parallel to the channel length.

approximately 15% in OFETs with the channel length aligned parallel to the trenches, compared to W with an unstructured gate insulator surface. Conversely, the effective OFET L is approximately 15% longer in OFETs with the channel length aligned perpendicular to the trenches, compared to L with an unstructured gate insulator surface.

The output characteristics in Fig. 3(a) are shown for a gate-source bias (V_{GS}) of −40 V; in Fig. 3(b), the output characteristics with varying V_{GS} are shown for a OFET with trenches aligned parallel to L. Output characteristics with L parallel to the trenches exhibit a significantly higher I_D than OFETs with L perpendicular to the trenches. Both parallel and perpendicularly aligned OFETs demonstrate ohmic source and drain contact behavior, although parasitic gate and film leakage currents are observed in the small offset of the drain current (I_D) for small values of the drain-source bias (V_{DS}). Similarly, the linear regime ($V_{DS}=-5$ V) transfer characteristics shown in Fig. 4 also display a higher I_D with L parallel to the trenches than for perpendicular alignment. No correlation is observed in the off-state current or subthreshold slope (S), as seen in Fig. 4. For the results shown in Fig. 4, a charge carrier field-effect mobility at $V_{GS}=-40$ V of 2.0×10^{-3} cm^2/V s was extracted for trenches parallel to L ($\mu_{FE}^{\parallel}$); for trenches aligned perpendicular to L, $\mu_{FE}^{\perp}=2.5\times10^{-4}$ cm^2/V s. In the results examined here, this produces a mobility anisotropy ratio of $\mu_{FE}^{\parallel}/\mu_{FE}^{\perp}=8.1$; the field-effect mobility anisotropy ratio was found to vary from 3 to 8 for different OFET samples. Threshold voltage variation with channel alignment to the trenches was

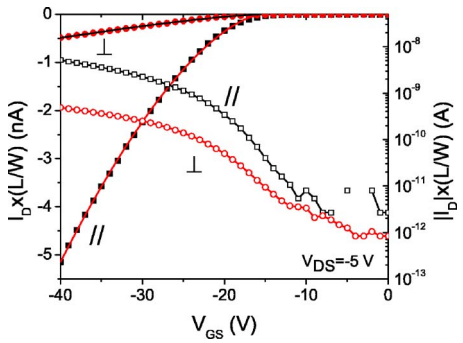

FIG. 4. (Color online) Transfer characteristics of TBP OFETs on nanostructured SiO_2. Lines connecting data points indicate the fit of the transfer characteristics. Open markers indicate the semilog scale plot, with lines connecting data points to aid viewing. I_D for both devices has been normalized to W/L.

negligible: $V_T^{\parallel}=-15.3$ V and $V_T^{\perp}=-15.4$ V. Variation in μ_{FE} with orientation of the OFET channel to the trenches (and ordered TBP aggregates), but not in V_T or S, suggests that the electronic structure of the dendrites in the trenches, is similar to that of an unstructured thin film, but that the introduction of a thin, highly ordered region of TBP aggregates across the OFET channel length provides a better defined conduction pathway for holes. While no trend was observed for V_T, the typical μ_{FE} for unpatterned, control substrates was, in the linear regime, half that observed for patterned samples with perpendicular groove alignment, and one order of magnitude less than that observed for patterned samples parallel groove alignment. However, the off-state current and S were similar.

The thermal conversion of a precursor-route organic semiconductor was exploited by patterning the gate dielectric surface to enhance OFET performance through a preferred crystallization process at the gate insulator surface. AFM measurements showed that TBP crystallized preferentially along trenches formed in the gate insulator surface by laser interference lithography, thereby controlling the position and geometry of arrays of TBP aggregates over a large area with precise long-range order at the TBP/SiO_2 interface. OFETs displayed anisotropic charge carrier field-effect mobility, with larger field-effect mobility appearing in OFETs with ordered aggregates grown in the channel length direction than in OFETs with ordered aggregates grown perpendicular to the channel length direction.

[1] H. Sirringhaus, Adv. Mater. (Weinheim, Ger.) **17**, 2411 (2005).
[2] A. Facchetti, M.-H. Yoon, and T. J. Marks, Adv. Mater. (Weinheim, Ger.) **17**, 1705 (2005).
[3] M. Ofuji, K. Inaba, K. Omote, H. Hoshi, Y. Takanishi, K. Ishikawa, and H. Takezoe, Jpn. J. Appl. Phys., Part 1 **42**, 7520 (2003).
[4] H. Heil, T. Finnberg, N. von Malm, R. Schmechel, and H. von Seggern, J. Appl. Phys. **93**, 1636 (2003).
[5] L. Kinder, J. Kanicki, and P. Petroff, Synth. Met. **146**, 181 (2004).
[6] Y. Ueda, T. Kuriyama, T. Hari, and M. Ashida, J. Electron Microsc. **43**, 99 (1994).
[7] A. M. van de Craats, N. Stutzmann, O. Bunk, M. M. Nielsen, M. Watson, K. Mullen, H. D. Chanzy, H. Sirringhaus, and R. H. Friend, Adv. Mater. (Weinheim, Ger.) **15**, 495 (2003).
[8] S. Aramaki, Y. Sakai, R. Yoshiyama, K. Sugiyama, N. Ono, and J. Mizuguchi, Proc. SPIE **5522**, 27 (2004).
[9] P. B. Shea, A. R. Johnson, J. Kanicki, and N. Ono, IEEE Trans. Electron Devices **52**, 1497 (2005).
[10] P. B. Shea, L. R. Pattison, M. Kawano, J. Kanicki, P. Petroff, H. Yamada, and N. Ono, J. Appl. Phys. **100**, 034502 (2006).
[11] P. B. Shea, L. R. Pattison, M. Kawano, C. Chen, J. Chen, P. Petroff, D. C. Martin, H. Yamada, N. Ono, and J. Kanicki, Synth. Met. **157**, 190 (2007).
[12] S. Ito, T. Murashima, H. Uno, and N. Ono, Chem. Commun. (Cambridge) **1998**, 1661.
[13] S. Ito, N. Ochi, T. Murashima, H. Uno, and N. Ono, Heterocycles **52**, 399 (2000).
[14] Y. Shimizu, Z. Shen, T. Okujima, H. Uno, and N. Ono, Chem. Commun. (Cambridge) **2004**, 374.
[15] L. K. Pattison, Ph.D. thesis, University of California-Santa Barbara, 2006.
[16] F. Mallamace, L. M. Scolaro, A. Romeo, and N. Micali, Phys. Rev. Lett. **82**, 3480 (1999).
[17] M. A. Castriciano, A. Romeo, V. Villari, N. Micali, and L. M. Scolaro, J. Phys. Chem. B **107**, 8765 (2003).
[18] A. D. Schwab, D. E. Smith, C. S. Rich, E. R. Young, W. F. Smith, and J. C. de Paula, J. Phys. Chem. B **107**, 11339 (2003).
[19] R. Rotomskis, R. Augulis, V. Snitka, R. Valiokas, and B. Liedberg, J. Phys. Chem. B **108**, 2833 (2004).
[20] S. R. J. Brueck, Proc. IEEE **93**, 1704 (2005).
[21] M. C. Hamilton, S. Martin, and J. Kanicki, Chem. Mater. **16**, 4699 (2004).
[22] V. I. Klykov, N. N. Sheftal, and E. Hartmann, Acta Phys. Acad. Sci. Hung. **47**, 167 (1979).